CHALMERS
UNIVERSITY OF TECHNOLOGY

Pump Frequency Allocation and Dispersion Effect on Dual-Pump Phase Sensitive Amplifier Gain Spectrum

Citation for the original published paper (version of record):
Udayanga, R., Chen, J., Larsson, R. et al (2025). Pump Frequency Allocation and Dispersion Effect on Dual-Pump Phase Sensitive Amplifier Gain
Spectrum. IEEE Photonics Technology Letters, 37(22): 1273-1276.
http://dx.doi.org/10.1109/LPT.2025.3594193

(article starts on next page)

Pump Frequency Allocation and Dispersion Effect on Dual-Pump Phase Sensitive Amplifier Gain Spectrum

Ruwan U. Weerasuriya, *Senior Member, IEEE*, Junda Chen, Rasmus Larsson, and Peter A. Andrekson, *Fellow, IEEE*

***Abstract*—Dual-pump fiber optical parametric amplifiers offer wide, flat gain spectra across arbitrary wavelengths, often outperforming the use of single-pump designs. However, gain flatness depends on the pump frequencies' center of gravity relative to the nonlinear fiber's zero-dispersion wavelength. This study experimentally investigated the gain, gain flatness, and noise figure of degenerate dual-pump fiber-optic phase-sensitive amplification at various separations between these points. We demonstrated 38 dB gain with 1.5 dB gain flatness variation over a 30 nm bandwidth as well as a noise figure below the conventional 3 dB quantum limit for a degenerate signal.**

***Index Terms*—Phase-sensitive amplification, gain flatness, noise figure, stimulated Brillouin scattering, highly nonlinear fiber, four-wave mixing, fiber-optic parametric amplifier.**

I. Introduction

OPTICAL amplifiers play a crucial role in scientific and engineering applications, including optical communication, imaging, sensing, and spectroscopy [1]. They come in various types, each with advantages and limitations, making the choice application-dependent. Some amplifiers, like erbium-doped fiber amplifiers (EDFAs), use optically pumped rare-earth-doped fibers, while others rely on electrically pumped semiconductors [2]. These amplifiers achieve gain through population inversion and stimulated emission.

Alternatively, optical amplification can occur via nonlinear effects in fibers, such as stimulated Raman scattering and stimulated Brillouin scattering [1], [3]. Higher-order nonlinear effects, like the Kerr effect, enable optical parametric amplification (OPA) [3], [4] through three-wave or four-wave mixing (FWM) in materials such as $LiNbO_3$ [5], [6] or silica fiber [3]. The optical pump wavelength placement and waveguide dispersion in OPAs, determine the gain spectrum and its quality.

Depending on the operating mechanism, the amplification region may be confined to a limited gain bandwidth (e.g., EDFA) [2], [3]. Fiber optical parametric amplifiers (FOPAs), meanwhile, can amplify and process optical signals beyond conventional rare-earth-doped bands, extending optical communication to multiple telecommunication bands [3], [7]. Their performance is further enhanced when implemented as phase-sensitive amplifiers (PSAs), as the noise figure (NF) in theory can reach 0 dB. The dual-pump FOPA configuration is useful, as it enables flat gain and can operate in either degenerate or non-degenerate configurations, each suited for specific applications [4], [8], [9].

Recently, a dual-pump degenerate PSA was demonstrated, and its operational range was evaluated concerning the pump phase mismatch used for SBS suppression [10]; however, one of the most prominent parameters of gain flatness was not analyzed. Therefore, we further investigate its ability to achieve higher gain and improved gain flatness by analyzing the effect of dispersion parameters of the highly nonlinear fiber (HNLF). Additionally, we assess the impact on the noise figure of degenerate PSA at each tested point.

In this manuscript, Section II outlines the theory for gain and gain flatness and simulation results, Section III details the experimental setup, Section IV presents the experimental results, and Section V concludes the study.

II. Gain and Flatness Dependence

Key factors in choosing an optical amplifier, which are important when amplifying multiple wavelengths, are gain, gain flatness, and NF [1], [2]. Most commercially available optical amplifiers do not inherently provide flat gain but can be achieved through multi-wavelength pumping in Raman amplification [11], [12].

With a gain bandwidth exceeding 80 nm [9], and a low NF, FOPAs (or PSA) can provide better performance in terms of gain flatness and bandwidth control [13]. Moreover, a dual-pump FOPA offers an even broader and more uniform gain spectrum. This is achieved by optimizing phase-matching conditions and strategically selecting pump wavelengths relative to the zero-dispersion wavelength (ZDW). Compared to single-pump configurations, dual-pump FOPAs offer an additional independent parameter that enhances gain optimization and spectrum flatness, i.e., the pump separation, in addition to the center of gravity (CG) of the pump frequencies (ω_c).

The interacting waves' phase-matching condition primarily determines a FOPA (or PSA) gain. Each wave's phase depends on the medium's dispersion parameters (β^i). The linear phase mismatch in a dual-pump FOPA (or PSA) is given by [3] and [4]:

$$\Delta\beta = \beta(\omega_s) + \beta(\omega_i) - \beta(\omega_{p1}) - \beta(\omega_{p2}). \quad (1)$$

Received 11 June 2025; revised 17 July 2025; accepted 25 July 2025. Date of publication 30 July 2025; date of current version 15 August 2025. This work was supported by the Swedish Research Council (Vetenskapsrearc) under Grant VR-2015-00535. *(Corresponding author: Ruwan U. Weerasuriya.)*

The authors are with the Department of Microtechnology and Nanoscience, Chalmers University of Technology, 412 96 Gothenburg, Sweden (e-mail: ruwan.udayanga@chalmers.se).

Color versions of one or more figures in this letter are available at https://doi.org/10.1109/LPT.2025.3594193.

Digital Object Identifier 10.1109/LPT.2025.3594193

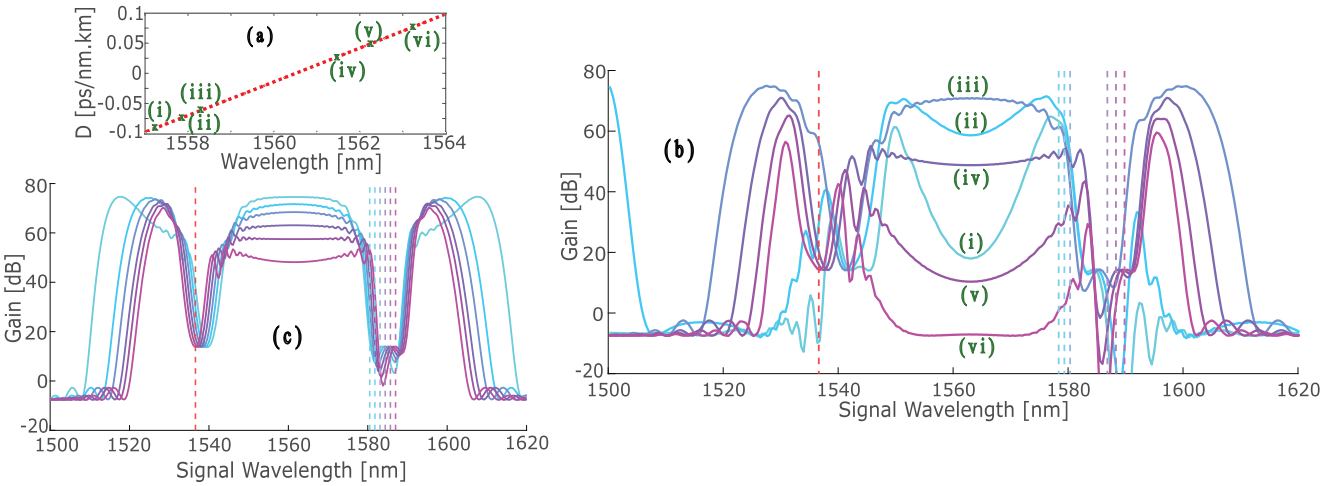

Fig. 1. (a) Dispersion profile of the HNLF. (b) Simulated gain Spectrum variation for different CGs as indicated in (a). (c) gain Spectrum variation for CGs selected between (iii) and (iv) as indicated in (a), Dashed vertical lines indicate the pump positions.

where, $\beta(\omega_k)$, is the propagation constant at angular frequency k, k are signal (s), idler (i), pump 1 (p1) and pump 2 (p2), respectively.

If we define the center of gravity of the pumps as $\omega_c = (\omega_{p1} + \omega_{p2})/2$, $\Delta\omega_s = (\omega_s - \omega_c)$ and $\Delta\omega_p = (\omega_{p1} - \omega_c) = (\omega_c - \omega_{p2})$, as described in [3], eq. 1 can be written as,

$$\Delta\beta = 2\sum_{m=1}^{\infty} \frac{\beta^{(2m)}}{(2m)!}[(\Delta\omega_s)^{2m} - (\Delta\omega_p)^{2m}]. \quad (2)$$

Here, the coefficients β^i are the Taylor terms of the propagation constant expanded around the CG, showing that phase mismatch depends mainly on even-order dispersion. When limited to the first two terms (up to fourth-order), Eq. 2 simplifies to

$$\Delta\beta = \beta^{(2)}[(\Delta\omega_s)^2 - (\Delta\omega_p)^2] + \frac{\beta^{(4)}}{12}[(\Delta\omega_s)^4 - (\Delta\omega_p)^4]. \quad (3)$$

In our case, we implement and experiment with the degenerate dual-pump PSA scheme configuration. Therefore, we can assume that $\Delta\omega_s \simeq 0$, so that equation 3 can be rewritten,

$$\Delta\beta(\Delta\omega_s \simeq 0) = -\left[\beta^{(2)}(\Delta\omega_p)^2 + \frac{\beta^{(4)}}{12}(\Delta\omega_p)^4\right]. \quad (4)$$

Equation 4 implies that the gain variation mainly depends on the β^2 and β^4 parameters of the nonlinear media used. The dispersion parameters at the CG mainly represent the dispersion parameters of the pumps. Therefore, the placement of the CG with respect to the zero dispersion wavelength (λ_0) will have an impact on the gain and its profile. During the experiments, we swept the L-band pump location, thus changing the $\Delta\omega_p$ parameter and CG simultaneously.

For comparison, we also investigated this sweep numerically. From available data, we estimated the dispersion characteristics (beta parameters) of the highly nonlinear fiber (HNLF) for the CG points around λ_0 that matches the L-band pump sweep, see Fig. 1(a).

In the simulations, the C-band pump was fixed at 1536.6 nm, and the L-band pump was varied, both with powers of 0.5 W. The HNLF parameters used were: 1.1 dB/km loss, 25 $W^{-1}km^{-1}$ nonlinearity, 350 m length, and λ_0 = 1561.7 nm.

To study the impact on gain and the gain spectrum, we performed simulations by selecting CGs between 1557 nm and 1564 nm in 0.5 nm steps. However, only six representative CG values were chosen to capture the most significant variations of interest. These selected CGs are shown in Fig.1(a).

As illustrated in Fig.1(b), the shape of the gain spectrum is primarily influenced by the placement of the CG relative to the ZDW, or, equivalently, by the effective dispersion parameters (β^i) corresponding to each CG. This indicates that by carefully selecting the CG or pump frequency placement, it is possible to operate the amplifier in a region with flat gain. A relatively flat gain region was identified between CG points (iii) and (iv), as highlighted in Fig.1(b).

To further examine the gain flatness between CG points (iii) and (iv) in Fig. 1(a), six additional CG values were selected within that range. A gradual transition toward a flatter gain response was observed and is depicted in Fig.1(c). As shown, gain flatness can be achieved along with a simultaneous increase in gain. However, this behavior is bounded and does not continue indefinitely, as evidenced in Fig.1(b). Further details on the relationship between CG positioning, dispersion, and their role in enhancing gain and achieving gain flatness can be found in [3] and [7].

III. Experimental Configuration

The experimental setup is shown in Fig.2. A seed for the L-band pump was generated using an electro-optic (EO) comb with a 25 GHz free spectral range, driven by a narrow-linewidth laser. A selected EO comb line was split: one part was injection-locked to a DFB laser to preserve the linewidth and enhance the optical signal-to-noise ratio (OSNR), and then used in two FWM-based wavelength-conversion stages to produce the L-band pump. The other part was directed to a separate FWM-based wavelength-conversion stage to generate the signal wavelength.

Both pump waves were individually phase-modulated using three RF tones (95 MHz, 305 MHz and 490 MHz) to suppress stimulated Brillouin scattering. The phase-modulated pumps

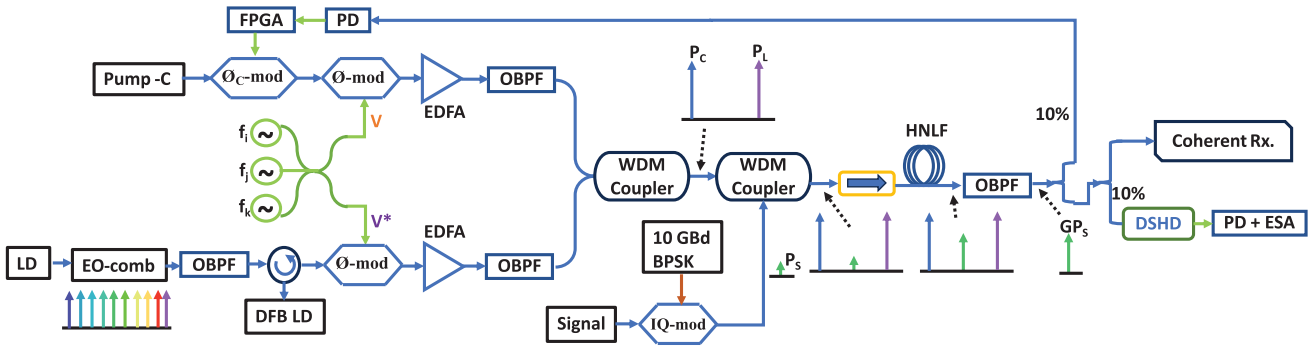

Fig. 2. Simplified experimental setup. Polarization controllers were used to align the polarization of all waves at all points. WDM, wavelength-division multiplexer; OBPF, optical band-pass filter; PM, power meter; PD, photo-detector; FPGA, field programmable gate array. ϕ-mod /ϕ_c-mod, electro-optic phase modulator, ESA, electrical spectrum analyser.

were then amplified, optically filtered, and combined using a WDM coupler.

A 10 Gbaud binary phase-shift keyed (BPSK) signal was generated using the other power-splitted seed of the EO comb line and combined with the pumps. The combined signal and pumps were launched into a highly nonlinear fiber (HNLF) for amplification. At the output of the HNLF, the BPSK signal was optically filtered. A portion (10%) of the filtered signal was used to control the phase of the C-band pump, enabling phase-sensitive amplification. The remaining 90% was directed to bit-error rate (BER) measurements and idler analysis. Much of the setup follows the configurations described in [10] and [14], where further details on experimental optimization and data collection can be found. A key distinction is that the choice of the CGs in the normal dispersion region of the HNLF was constrained by the bandwidth and cutoff response of the WDM coupler (1558.90 nm).

IV. Results and Discussion

This work investigates how the placement of the CG relative to λ_0 influences gain and its spectral profile. The HNLF gain was estimated from the optical spectrum analyser (OSA)-captured spectrum as $G = (P_{r,\mathrm{OSA}} - P_{n,\mathrm{OSA}})/2P_r$, where P_r is the input signal power to the HNLF, $P_{r,\mathrm{OSA}}$ is the power at the signal wavelength in the OSA spectrum, and $P_{n,\mathrm{OSA}}$ is the power of the amplified vacuum noise at the same wavelength. The factor of 2 accounts for the presence of both signal and idler components, isolating the signal contribution for consistency with non-degenerate gain definitions.

Due to limitations imposed by the WDM coupler at the input of the PSA, we selected 10 different CG wavelengths between 1558.5 nm and 1562.5 nm, using 0.4 nm steps to align with the spacing of the EO comb. To ensure clearer visualization and better spacing between the spectral curves, only seven representative output spectra were selected to capture the most significant variations in gain and gain spectrum. As shown in Fig.3, a flat gain was achieved about CG $\approx$ (λ_0 - 0.7 nm). Further detuning increased gain while maintaining flatness up to a point, limited by the WDM coupler's bandwidth, which is also reflected in the BER measurements. At CG $\approx$ (λ_0 - 3.0 nm) the gain fluctuation remained within 1.5 dB over a 30 nm range (inset of Fig.3). We couldn't observe the flatness degradation beyond optimal detuning as evident in Fig.1 (b) due to the limitation of the WDM coupler bandwidth,

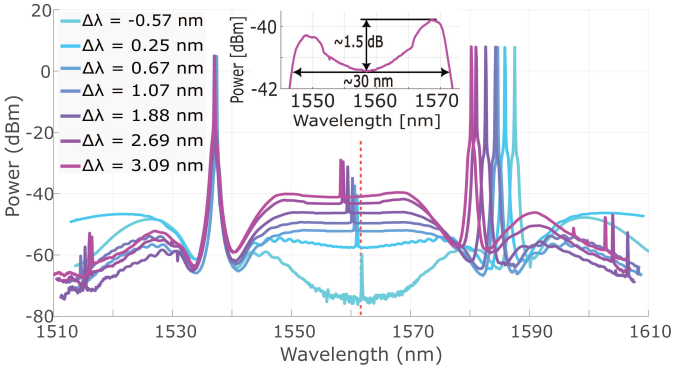

Fig. 3. Measured PSA output spectra for different CGs captured with 0.1 nm resolution at 1% tap after the HNLF. A red dashed line depicts ZDW (λ_0). $\Delta\lambda$ = (λ_0 - λ_{CG}). The inset is an expanded spectrum part for $\Delta\lambda$ = 3.09 nm without BPSK signal.

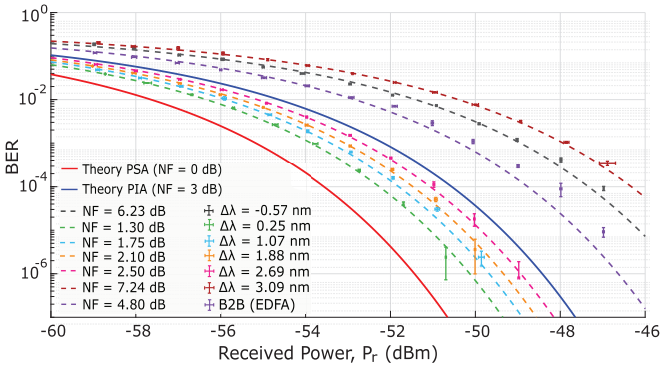

Fig. 4. BER vs. received power for the BPSK-signal for some selected $\Delta\lambda$ of the PSA performance. Dashed lines indicate the theoretical NF values, which were mapped to the experimental results.

underscoring the importance of pump placement or dispersion profile in optimizing dual-pump PSA performance.

Beyond spectral analysis, a more comprehensive characterization was performed by measuring the bit-error rate (BER) for a 10 Gbaud BPSK signal in a degenerate PSA configuration. The BER values as a function of received signal power are presented in Fig.4. The performance was assessed for ten different CGs, however, only six selected CGs are plotted to represent the full range of interest adequately. As shown in Fig.4, the PSA can operate below the conventional 3 dB quantum limit with a $\Delta\lambda$ = 2.69 nm. There were two outlier CG wavelengths observed: at $\Delta\lambda$ = −0.57 nm and $\Delta\lambda$ = 3.09 nm.

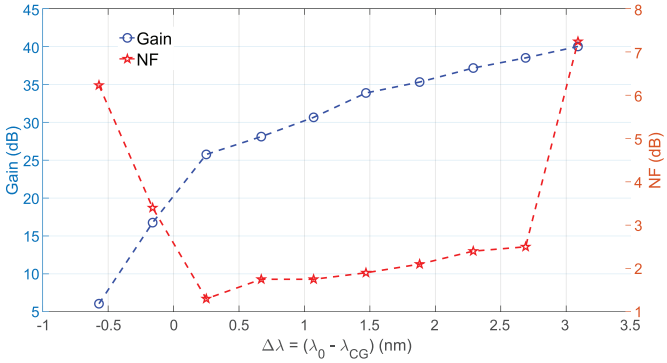

Fig. 5. Gain and theoretically mapped NF variation for different CG.

The higher BER deviation at $\Delta\lambda = 3.09$ nm is primarily attributed to operating at the very edge of the WDM coupler's bandwidth. Otherwise, a similar performance to the $\Delta\lambda = 2.69$ nm scenario could be expected. For the $\Delta\lambda = -0.57$ nm case, the degraded performance is mainly due to the low gain observed. Except for these two cases, all other CGs operated below the theoretical noise figure (NF) value of 2.5 dB.

Fig.5 illustrates the PSA gain for different CG positions along with the corresponding theoretically mapped NF. As observed in Fig.5, the dual-pump degenerate PSA can operate well below the quantum limit of 3 dB, achieving more than 20 dB gain. The NF variation between $\Delta\lambda = 0.25$ nm and 2.69 nm is mainly due to increased idler presence outside the pump band, as shown in Fig. 3. These idlers introduce noise into the signal during continuous parametric amplification along the HNLF, degrading the NF. As discussed above, the CGs at $\Delta\lambda = -0.57$ nm and $\Delta\lambda = 3.09$ nm exhibit higher NF penalties. However, the performance at the $\Delta\lambda = 3.09$ nm could be brought below the quantum limit with the implementation of a more suitable WDM coupler in the setup.

V. Conclusion

We have experimentally demonstrated a dual-pump PSA featuring a flat gain profile over a 30 nm bandwidth and a gain of approximately 40 dB, which operates well below the quantum limit (3 dB) in the degenerate signal case and is capable of multi-wavelength amplification based on four-wave mixing (FWM). Despite its advantages, the implemented PSA scheme has inherent limitations, primarily due to SBS and the optical phase-locked loop (OPLL). The phase modulation scheme employed to suppress SBS introduces its own penalties and, the OPLL's performance is affected by its bandwidth, signal-to-noise ratio (SNR), loop delay, and the pump lasers' phase noise bandwidth [10], [14]. These factors degrade system performance, particularly when aiming for lower NF values. The NF performance can be further enhanced by employing WDM couplers with lower insertion loss as well as minimizing any splice losses in the HNLF.

As an alternative to our approach, keeping the pump separation constant while varying the CG may allow for even broader gain bandwidth and higher gain, without sacrificing gain flatness. However, this method requires careful optimization of the dispersion parameters, as even small variations in higher-order dispersion can severely disrupt gain flatness and magnitude. With proper design, a dual-pump PSA can function as a high-gain, broadband amplifier with a flat response.

Moving toward practical implementation, integrating the dual-pump PSA into a chip-based platform offers significant advantages [5], [6], [15]. Such an approach would inherently eliminate SBS issues and remove the need for ultra-low-noise pump lasers, by reducing OPLL loop delay. These improvements and advancements may open a wide range of application opportunities for dual-pump PSAs, not only in multi-wavelength amplification but also in ultra-sensitive reception in optical free-space communication systems [16], optical sensing [17], and quantum metrology [18].

References

[1] G. P. Agrawal, *Nonlinear Fiber Optics*, 6th ed., New York, NY, USA: Academic, 2019.
[2] E. Desurvire, *Erbium-Doped Fiber Amplifiers: Principles and Applications*, 1st ed., Hoboken, NJ, USA: Wiley, 1994.
[3] M. E. Marhic, *Fiber Optical Parametric Amplifiers, Oscillators and Related Devices*. Cambridge, U.K.: Cambridge Univ. Press, 2007.
[4] P. A. Andrekson and M. Karlsson, "Fiber-based phase-sensitive optical amplifiers and their applications," *Adv. Opt. Photon.*, vol. 12, no. 2, pp. 367–428, 2020.
[5] Z. Yan et al., "χ^2-based AlGaAs phase sensitive amplifier with record gain, noise, and sensitivity," *Optica*, vol. 9, no. 1, p. 56, Jan. 2022.
[6] K. J. Lee et al., "Phase sensitive amplification based on quadratic cascading in a periodically poled lithium niobate waveguide," *Opt. Exp.*, vol. 17, no. 22, pp. 20393–20400, Oct. 2009.
[7] M. E. Marhic, F. S. Yang, L. G. Kazovsky, and Y. Park, "Broadband fiber-optical parametric amplifiers and wavelength converters with low-ripple Chebyshev gain spectra," *Opt. Lett.*, vol. 21, no. 17, pp. 1354–1356, 1996.
[8] C. J. McKinstrie and S. Radic, "Parametric amplifiers driven by two pump waves with dissimilar frequencies," *Opt. Lett.*, vol. 27, no. 13, pp. 1138–1140, 2002.
[9] J. M. Chavez Boggio, C. Lundstrom, J. Yang, H. Sunnerud, and P. A. Andrekson, "Double-pumped FOPA with 40 dB flat gain over 81 nm bandwidth," in *Proc. 34th Eur. Conf. Opt. Commun.*, Jul. 2008, pp. 1–2.
[10] R. U. Weerasuriya, R. Larsson, and P. A. Andrekson, "Effect of counter-phase pump modulation of phase-sensitive amplifiers noise performance and SBS suppression," *Opt. Exp.*, vol. 33, no. 7, pp. 16174–16186, Apr. 2025.
[11] M. N. Islam, "Raman amplifiers for telecommunications," *IEEE J. Sel. Top. Quantum Electron*, vol. 8, no. 3, pp. 548–559, Mar. 2002.
[12] H. Masuda, A. Mori, K. Shikano, and M. Shimizu, "Design and spectral characteristics of gain-flattened tellurite-based fiber Raman amplifiers," *J. Lightw. Technol.*, vol. 24, no. 1, pp. 504–515, Jan. 2006.
[13] L. Provino, A. Mussot, E. Lantz, T. Sylvestre, and H. Maillotte, "Broadband and flat parametric amplifiers with a multisection dispersion-tailored nonlinear fiber arrangement," *J. Opt. Soc. Amer. B, Opt. Phys.*, vol. 20, no. 7, pp. 1532–1537, 2003.
[14] R. Larsson, R. U. Weerasuriya, and P. A. Andrekson, "Ultralow-noise preamplified optical receiver using conventional single-wavelength transmission," *Optica*, vol. 11, no. 11, pp. 1497–1502, Nov. 2024.
[15] P. Zhao, V. Shekhawat, M. Girardi, Z. He, V. Torres-Company, and P. A. Andrekson, "Ultra-broadband optical amplification using nonlinear integrated waveguides," *Nature*, vol. 640, no. 8060, pp. 918–923, Apr. 2025.
[16] R. Kakarla, J. Schröder, and P. A. Andrekson, "One photon-per-bit receiver using near-noiseless phase-sensitive amplification," *Light, Sci. Appl.*, vol. 9, no. 153, pp. 1–7, 2020. [Online]. Available: https://doi.org/10.1038/s41377-020-00389-2
[17] F. Hudelist, J. Kong, C. Liu, J. Jing, Z. Y. Ou, and W. Zhang, "Quantum metrology with parametric amplifier-based photon correlation interferometers," *Nature Commun.*, vol. 5, no. 1, p. 3049, Jan. 2014.
[18] M. A. Butt, G. S. Voronkov, E. P. Grakhova, R. V. Kutluyarov, N. L. Kazanskiy, and S. N. Khonina, "Environmental monitoring: A comprehensive review on optical waveguide and fiber-based sensors," *Biosensors*, vol. 12, no. 11, p. 1038, Nov. 2022.
[19] R. U. Weerasuriya, "*Dataset—Pump frequency allocation and dispersion effect on dual-pump phase sensitive amplifier gain spectrum*," doi: 10.21227/4g9f-r630.